Transport in Porous Media (2006) 63: 323–347
DOI 10.1007/s11242-005-6870-0

Measurement and Modelling of Gas Condensate Flow Around Rock Perforation

M. JAMIOLAHMADY[1,⋆], A. DANESH[1], M. SOHRABI[1] and D. B. DUNCAN[2]
[1]*Institute of Petroleum Engineering, Heriot-Watt University, Edinburgh EH14 4AS, U.K.*
[2]*Department of Mathematics, Heriot-Watt University, Edinburgh EH14 4AS, U.K.*

(Received: 13 October 2004; accepted in final form: 3 May 2005)

Abstract. In the petroleum production industry wells are mostly cased and perforated in the producing formation. Perforation characteristics such as size, length, number of perforation tunnels and their arrangements as well as fluid and rock properties determine fluid flow behaviour in the wellbore region, hence, well productivity. Flow of gas and condensate around a perforation tunnel (including the damaged zone) has been studied by performing steady-state core experiments and simulating the results numerically, using a finite element modelling approach. The model allows for the changes in fluid properties and accounts for the coupling of the two phases and the inertial effect using a fractional flow based correlation. The results indicated that different sets of thickness-permeability ($h-k$) values obtained from matching single-phase flow performance could be assigned to the damaged zone around perforation to represent the two-phase flow performance. The status of the tip of the perforation for two extreme cases of totally closed and fully open was investigated and found to have a minimal effect on the performance of the system.

Key words: two-phase flow, gas-condensate, relative permeability, inertia, rate effect, perforation, perforated rock.

Nomenclature

D	non-Darcy coefficient (m).
h	thickness (m).
k	absolute permeability (m^2 or mD).
$k(S_{wi})$	permeability at S_{wi} (m^2 or mD).
k_e	effective permeability (m^2 or mD).
k_r	relative permeability.
L_c	core length (m).
L_p	perforation length (m).
P	pressure (Pa).
P_c	capillary pressure (Pa).
Q	flow rate ($m^3\,s^{-1}$).
r	radial dimension of radial coordinate system, (m^{-1}).

⋆Author for Correspondence: e-mail: Jami.Ahmady@pet.hw.ac.uk

R_c core radius (m^{-1}).
R_p perforation radius (m^{-1}).
S_{wi} immobile water saturation.
V velocity ($m\,s^{-1}$).
Y weight function for interpolation of k_r.
x_j weight fraction of component j in liquid.
y_j weight fraction of component j in gas.
z_j total weight fraction of component j in mixture.
z axial dimension of radial coordinate system (m^{-1}).

Greek symbols

β single-phase inertial factor (m^{-1}).
$\beta(S_{wi})$ single-phase inertial factor at S_{wi} (m^{-1}).
ϕ porosity of porous medium.
μ viscosity ($kg\,ms^{-1}$).
ρ density ($kg\,m^{-3}$).

Subscript

ave average value.
b base value.
cr crushed zone.
g gas phase.
in core inlet.
iner inertia included.
L liquid (i.e., condensate).
m miscible case.
meas measured value.
mod predicted value.
out core outlet.

Abbreviations

GTR gas fractional flow.
i-D i (i = 1–3) dimensional system.
IFT interfacial tension.
Exp experimental value of.
Mod predicted value.

Operators

|| absolute value.
Δ difference operator.
$\nabla.$ divergence operator.
∇ gradient operator.

1. Introduction

The fluid flow behaviour around cased and perforated wells is different from that around openhole completions. Considerable effort has been

directed towards understanding and modelling this subject by many investigators. Muskat (1943) presented the first analytical treatment of the problem in 1943 representing perforation tunnels as point sinks in his analysis. Other early investigators used finite difference modelling approaches to examine the flow in perforated completions (e.g., Harris, 1966; Hong, 1975; Bell *et al.*, 1972). Later investigators applied finite element methods, which model the geometry of the perforation with greater precision (e.g., Koltz *et al.*, 1974; Locke 1981; Tariq, 1987). Most of the practical perforated well productivity estimations for single-phase flow carried out today are based on Tariq's work (1987). However, there are some criticisms about the lack of generality (e.g., Ichara, 1987; Brooks, 1997; Dogulu, 1998) and accuracy of his results, especially at large perforation lengths and in the non-Darcy flow region (e.g., Behie and Settari, 1993; Jamiolahmady *et al.*, 2004).

Compared to single-phase flow, the problem of multi-phase flow in a perforation has received much less attention. The limited literature available on multi-phase flow in the perforated region usually involves major oversimplifications in representing the actual flow behaviour (e.g., Behie and Settari; 1993; Saleh and Stewart, 1996).

In gas condensate reservoirs the process of condensation around the wellbore, when the pressure falls below the dew point, creates a two-phase region in which the flow of gas and condensate phases is controlled by the viscous, capillary and inertial forces. The gas-condensate flow mechanisms in this near wellbore region are different from those of gas-oil and also gas-condensate in the reservoir bulk. The improvement of relative permeability of condensing systems at low interfacial tension (IFT) due to an increase in velocity, referred to as the "positive coupling effect", was first reported by Danesh *et al.* (1994). Since then many investigators have worked on this flow behaviour both experimentally (e.g., Henderson *et al.*, 1996; Chen *et al.*, 1997) and theoretically (Jamiolahmady *et al.*, 2000, 2003 and 2005). The coupling effect has also been shown to be in strong competition with that of inertia, which tends to reduce relative permeability at very high velocities (Henderson *et al.*, 2001). Jamiolahmady *et al.* (2003) have recently developed a generalised relative permeability correlation, which accounts for the opposing effects.

In this paper the governing equations describing the two-phase flow of gas and condensate around a perforation tunnel surrounded by a damaged zone are solved using the Femlab mathematical package (version 2.3, 2002), which is based on the finite-element method. The model allows for the changes in fluid properties and accounts for the combined effects of coupling and inertia on relative permeability of gas-condensate systems. It successfully simulates gas-condensate flow behaviour at different velocity and fractional flow values in unperforated sandstone and carbonate core samples as measured in the laboratory. It also reproduces, with reasonable accuracy, measured data in a perforated core sample when the damaged

zone is included in the simulation. The physical properties of the damaged zone are those estimated by matching the single-phase flow performance. The effect of the status of the tip of the perforation for two extreme cases of totally closed and fully open is also investigated. The results highlight the significance of relevant parameters affecting the perforation performance. In particular they are useful for simulating and comparing performances of open-hole and perforated wells.

2. Flow Measurements

A high-pressure core flood facility was used to measure the gas and condensate relative permeabilities by the steady state method. The core is saturated by the gas above its dew point pressure and then depleted to a selected pressure below the dew point allowing an initial condensate saturation to form by condensation. The gas and condensate, C1 and nC4 at 310 K, equilibrated at the test pressure are then injected simultaneously into the core at a constant gas volumetric fractional flow (GTR) at the test pressure. When the steady state conditions are achieved, the relative permeabilities of both phases are determined by using the flow rates and measured differential pressure across the core. The injection rates are then increased, at constant GTR, to detect the effect of velocity on relative permeability. The same procedure is repeated at lower GTR values to generate data over a wide saturation range. Further details on the test facility and experimental procedures can be found elsewhere (Henderson *et al.*, 1996).

Two core samples, Texas Cream, a carbonate rock and Clashach, a sandstone rock were used in this study. Clashach had a permeability of 553 md, porosity of 0.177 and single-phase inertial factor (β) of 1.035E8 m^{-1}. The corresponding values for the Texas cream core were 9.4 mD, 0.209 and 3.927E9 m^{-1}, respectively. Relative permeability measurements were conducted on the rock samples prior to perforating them. A single slim hole was drilled in the centre of the rock, with its dimensions relative to those of the core bulk selected such that the combined perforated and non-perforated sections simulate the flow characteristics in real cases, as closely as possible in a linear system. The Texas cream core sample had a radius of 2.495 cm and length, L_c, of 24.2 cm, which was then perforated by drilling a hole with $R_p = 0.6$ and $L_p = 15$ cm in it. The outlet of the core matrix was blanked off, allowing outflow only through the perforated hole. The perforation improved the rock permeability from 11 to 16.9 and from 550 to 870 mD for the Texas Cream and Clashach cores, respectively. Relative permeability measurements were carried out on both perforated rocks at IFT values of 0.15 and 0.85 mNm^{-1} corresponding to average pressure of 10.79 and 12.34 MPa, with velocities ranging from 6 to 725 $mday^{-1}$. These velocity values are the average total velocity, i.e., the total flow rate divided by the total pore area at the inlet to the core. Relative permeabilities are calculated

using Darcy's equation with the pressure difference across the core and the fluid properties at the average test pressure. The experimentally measured gas and condensate density values at P_{ave} of 10.79 and 12.34 MPa were 132.6 and 404.0 $kg\,m^{-3}$, respectively. The corresponding measured viscosity values were 0.0172 and 0.0601 mPa· s.

Figures 1 and 2 show the gas and condensate relative permeability measured for the Clashach core at seven velocities, for two IFT values of 0.85 and 0.15 $mN\,m^{-1}$, respectively. The velocities were calculated by dividing the total flow rate by the total pore area at the core inlet. The relative permeability variation with velocity is due to a combination of the coupling and inertial effects. At lower rates whereby inertia is not significant (i.e. velocities up to 56 md^{-1}) the increase in relative permeability with an increase in rate is evident at higher condensate to gas flow rate ratio (CGR). However at higher rates there is a decrease in relative permeability with an increase in rate at lower CGR due to inertia but the dominant effect of coupling is still evident at higher CGR. Similar observations are noted for measurements on the Texas Cream core, Figures 3 and 4.

3. Flow Simulation

The experiments were simulated numerically as follows.

3.1. GEOMETRY OF THE SYSTEM

The perforated porous medium is a homogenous core sample with absolute permeability k, length L_c and radius R_c. It has a perforated section with length L_p and radius R_p, Figure 5(a). The perforation was made by drilling a hole in the core and then sealing the rest of the core face to ensure that outflow was only through the perforation tunnel. The model was first used to simulate the experiments conduced on two un-perforated cores to confirm its integrity. The same set of equations written for a perforated core sample also applies to an un-perforated core sample and the only difference between the two models is the definition of their geometries and boundary conditions. Figure 5b shows the geometry of an un-perforated core. The boundary conditions for the two geometries are discussed below in Section 4.

3.2. MAIN ASSUMPTIONS

The main assumptions leading to the development of the models are as follows:

(1) The system is at steady-state conditions.

(1a) Mass transfer takes place between the two flowing phases as they travel through the porous medium but the total mass flowing in and out of the system is equal.

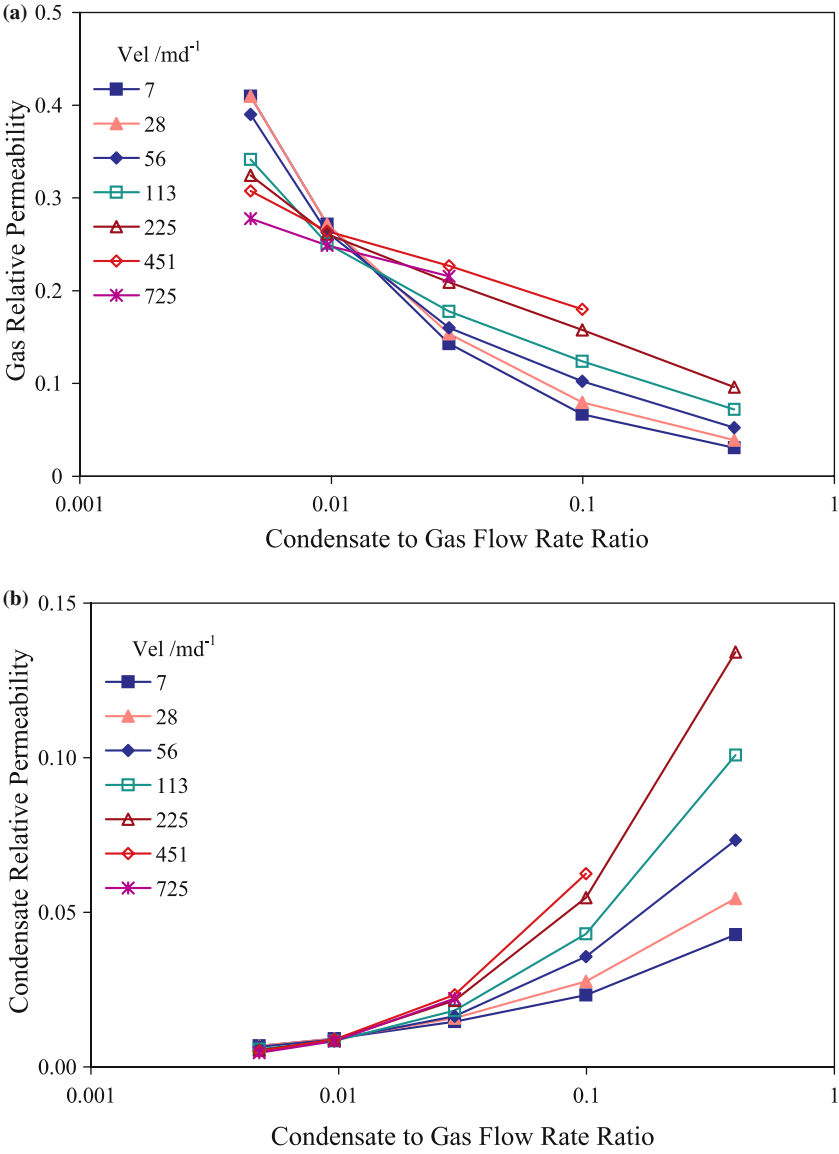

Figure 1. Measured relative permeability of perforated Clashach core at IFT = 0.85 mNm^{-1} and seven velocity levels for (a) gas (b) condensate.

(1b) The total mass flow rate of each component in the flowing mixture remains constant, that is, there is no chemical reaction in the core. This assumption does not prohibit local variations of total and individual components in place as saturations of gas and condensate phases change.

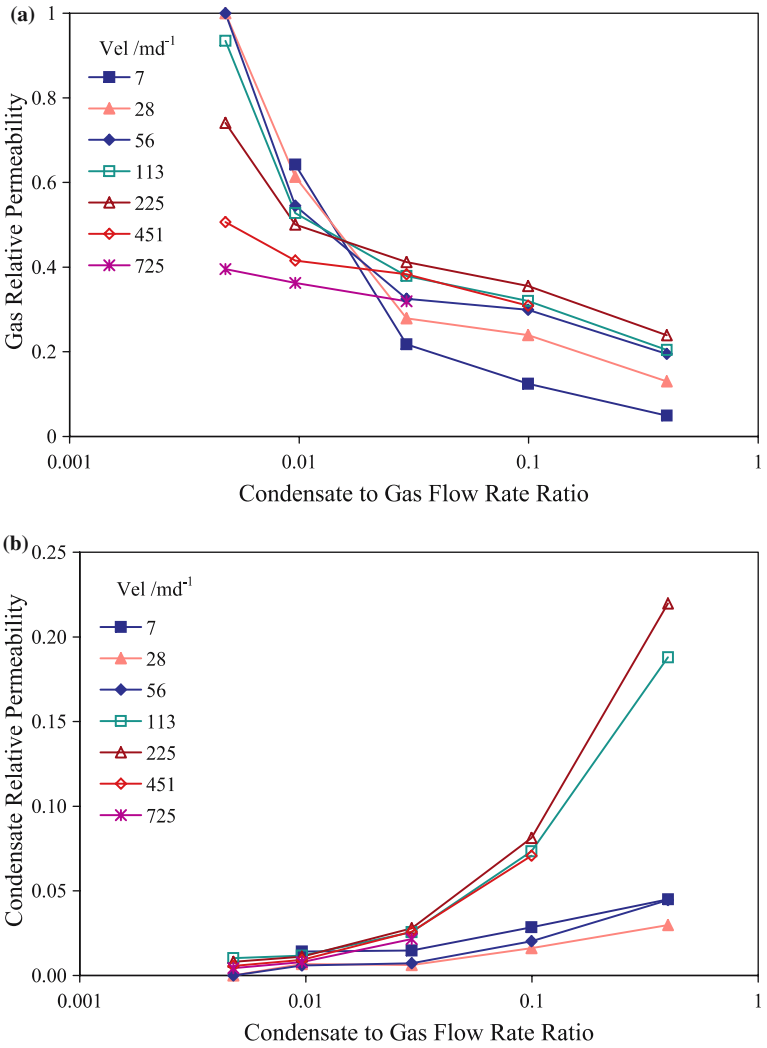

Figure 2. Measured relative permeability of perforated Clasach core at IFT = 0.15mNm^{-1} and seven velocity levels for (a) gas (b) condensate.

(1c) The flow rate of each phase, i.e., gas and condensate, varies with position but is fixed at any point in the system.
(2) The porous medium is homogenous.
(3) The phases are at thermodynamic equilibrium conditions.
(4) The system is isothermal.
(5) Gravitational segregation is minimal as the core was rotating during the experiments.
(6) Capillary pressure is neglected due to low gas-condensate IFT.
(7) Darcy's Law is extended to two-phase flow with relative permeability accounting for the velocity effects, i.e., coupling and inertial effects.

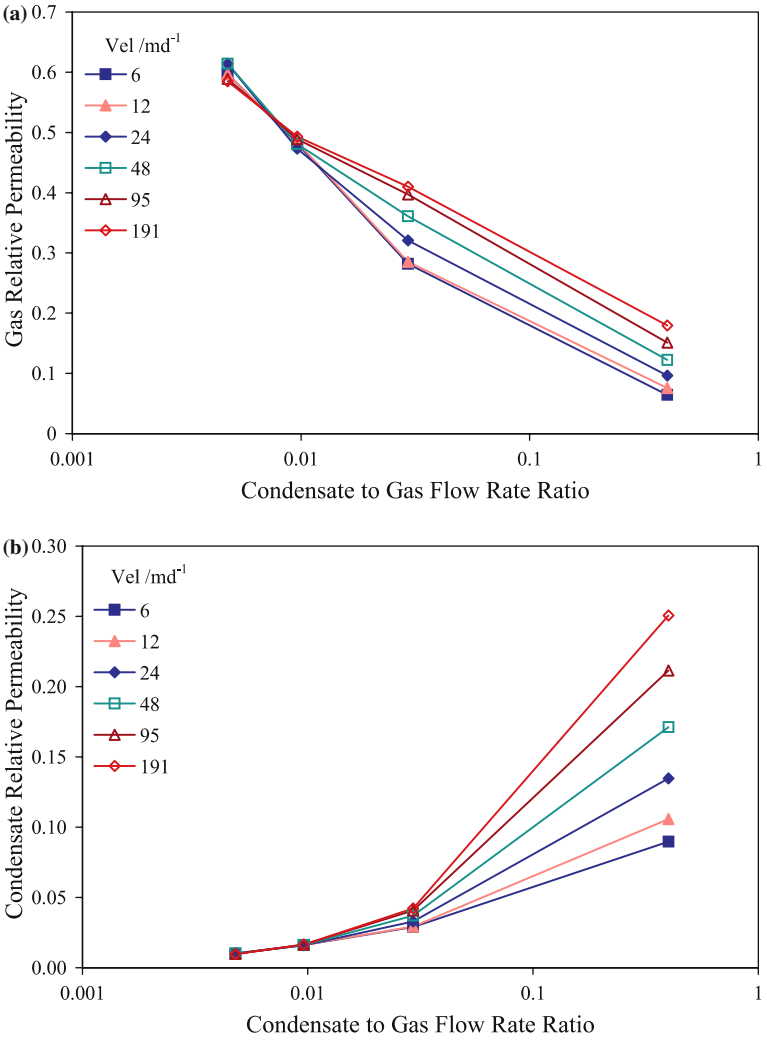

Figure 3. Measured relative permeability of perforated Texas Cream core at IFT = 0.85 m N m^{-1} and six velocity levels for (a) gas (b) condensate.

(8) The pressure inside the perforation tunnel is uniform due to its high conductivity compared to that of the porous medium. In a sensitivity study the viscous pressure drop across the perforation tunnel was calculated using the theory of homogenous flow in pipes and found to be minimal compared to that across the porous medium.

(9) Physical properties of damaged zone have been uniformly impaired due to the perforation process.

(10) The continuity of velocity and pressure at the boundary of this sub-domain with the main domain has been maintained.

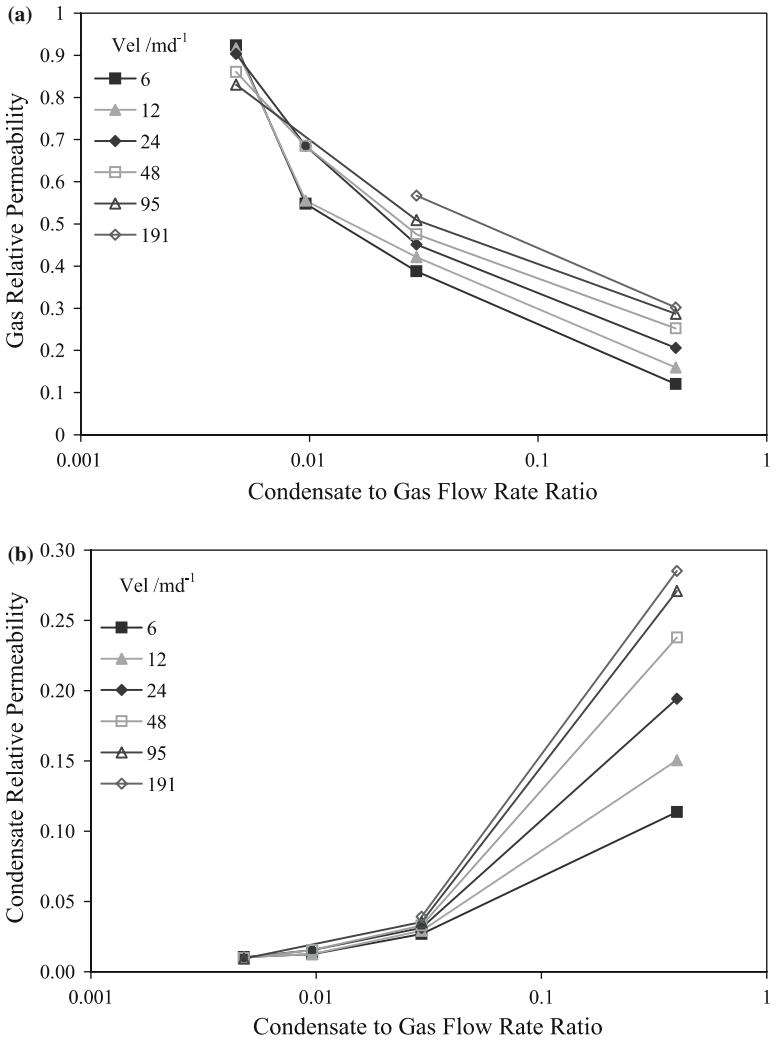

Figure 4. Measured relative permeability of perforated Texas Cream core at IFT $= 0.15\,\mathrm{mN\,m^{-1}}$ and six velocity levels for (a) gas (b) condensate.

3.3. BOUNDARY CONDITIONS

3.3.1. *Perforated Core*

The boundary conditions for the perforated core are

(1) Velocity of each phase at the inlet of the core is known and is the same over the entire inlet cross-sectional area of the core, $V_{\mathrm{in}} =$ known constant for all values of r at $z = 0$.

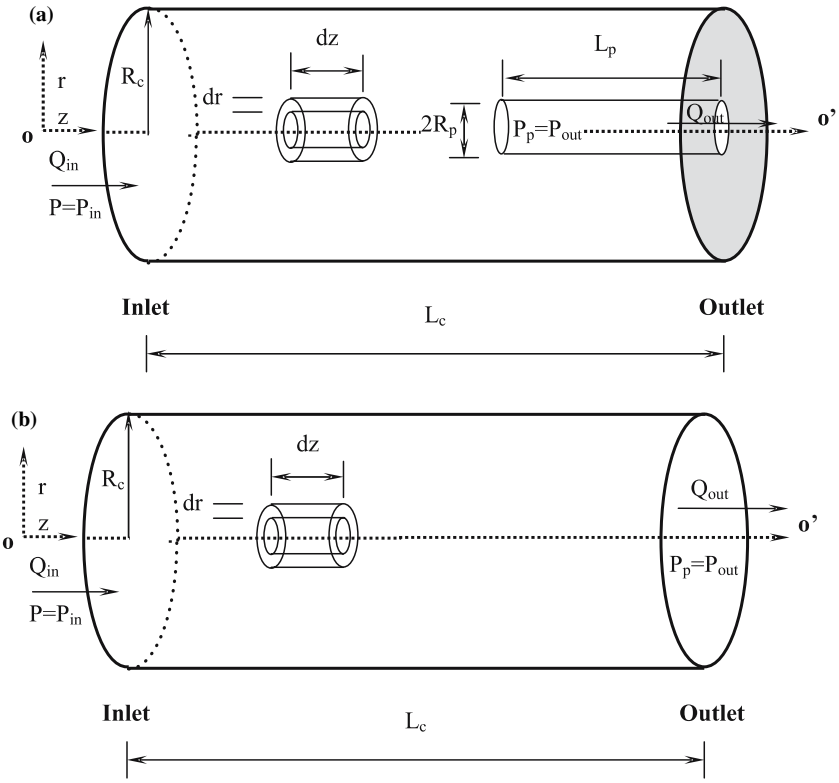

Figure 5. Geometry of the system in cylindrical co-ordinates (a) Perforated (b) unperforated core sample.

(2) No radial inflow or outflow at the outer surface of the core all along the core axis for both phases, i.e., $Q_g = Q_L = 0$ for all values of z at $r = R_c$.
(3) No outflow from the unperforated section of the core outlet, i.e., $Q_g = Q_L = 0$ for all values of $r > R_p$ at $z = L_c$.
(4) The value of pressure inside the perforation tunnel is known.

Due to the symmetry of flow around the core longitudinal axis, we solve the above problem for one half of the 2D cross-section of the core in the $(r - z)$ coordinate system. Therefore, there is an additional boundary condition of no flow crossing the longitudinal axis of the core in the vertical plane as shown in Figure 5(a).

In some of our sensitivity studies we have also evaluated the impact of the status of the perforation tip for two extreme case of fully open and totally closed. In the latter case the no flow boundary condition, similar to that of boundary condition number 3, was applied to the perforation tip surface.

3.3.2. *Un-Perforated Core*

The boundary conditions (1) and (2) are still applicable for an un-perforated core but boundary conditions (3) and (4) are replaced by a different boundary condition defined as,
(3) uniform pressure at the outlet end of the core, i.e., $P = P_{\text{out}}$ for any r at $z = L_{\text{c}}$.

3.4. GOVERNING EQUATIONS

The continuity equation in our system takes the following form:

$$\nabla.\left([\rho V]_{\text{g}} + [\rho V]_{\text{L}}\right) = 0, \tag{1}$$

where $\nabla.$ is divergence operator, ρ is the density, V is the velocity and subscripts (g) and (L) refer to gas and condensate (liquid), respectively.

Darcy's Law is extended to two-phase flow, assumption (7), as

$$\left[V = \frac{kk_{\text{r}}\nabla P}{\mu}\right]_j \quad j = L, g, \tag{2}$$

where ∇ is the gradient operator, P is the pressure, μ is the viscosity and k is the absolute permeability.

The relative permeability, k_{r}, in general is considered to be a function of velocity accounting for effects of inertia and coupling.

Substituting Equation (2) into Equation (1) and dividing by k leads to

$$\nabla.\left(\left\{\left[\frac{\rho k_{\text{r}}}{\mu}\right]_{\text{g}} + \left[\frac{\rho k_{\text{r}}}{\mu}\right]_{\text{L}}\right\}\nabla P\right) = 0. \tag{3}$$

Considering assumption (1b) we can write

$$z_j = \frac{\rho_{\text{g}} Q_{\text{g}} y_j + \rho_{\text{L}} Q_{\text{L}} x_j}{\rho_{\text{g}} Q_{\text{g}} + \rho_{\text{L}} Q_{\text{L}}} = \frac{\rho_{\text{g}}\text{GTR}\, y_j + \rho_{\text{L}}(1-\text{GTR})x_j}{\rho_{\text{g}}\text{GTR} + \rho_{\text{L}}(1-\text{GTR})} = \text{constant}, \tag{4}$$

where z_j, y_j and x_j are mass fraction of component j in the mixture, gas and liquid phases, respectively. Q is the volumetric flow rate and GTR is the gas fractional flow.

All the parameters in the equations presented here and implemented in the simulator are in consistent (SI) units.

3.5. FLUID PROPERTIES

The fluid properties of equilibrated phases of a fixed overall composition depend only on pressure at a given temperature. This also implies

that fractional flow is only a function of pressure at constant temperature, Equation (4). The fluid properties can be calculated using an equation of state based compositional model or just by simply relating them to pressure using empirical correlations. A binary mixture of C1 (methane) and *n*-C4 (normal butane) was used as a model gas-condensate fluid in the core experiments. The values of composition, density (ρ), viscosity (μ) and interfacial tension (IFT) of C1-*n*C4 mixtures measured in this laboratory as well as literature data (Sage *et al.*, 1940; SUPERTRAPP User's Guide, 1992; Weinaug and Katz, 1943) at 311 K over a wide pressure range were implemented in the model in a tabular form. The Hermite cubic spline interpolation sub-programme from the Matlab mathematical package (version 6.1, 2001) was used to obtain the data without oscillations.

3.6. RELATIVE PERMEABILITY

In Equation (3), gas relative permeability (k_{rg}) is estimated using a fractional flow based correlation developed recently (Jamiolahmady *et al.*, 2003). In this formulation k_{rg} is interpolated between a base curve and the miscible-fluids curve using an interpolation function Y_g, which also accounts for the effect of micro-pores. The base curve is measured at a high value of interfacial tension and low velocity (commonly measured data), which then is adjusted for the effect of inertia. The miscible gas relative permeability curve is also modified to include the inertial effect. The condensate relative permeability k_{rL} is related to k_{rg} by the definition of fractional flow. A summary of the formulation involved in this correlation can be found in Appendix A.

3.7. MATHEMATICAL SOLUTION TECHNIQUE

In the set of equations described in the previous sections, there is one main equation, Equation (3), and one auxiliary equation, Equation (4). Although all variables can be expressed in terms of pressure, we solve these two equations for pressure and gas fractional flow (GTR). That is, the fluid properties are only a function of pressure. The k_{rL} expression, Equation (A.3), involves P, GTR and k_{rg}. The interpolation for k_{rg}, Equation (A.1), requires a base curve k_{rgb}, a miscible curve k_{rgm} and the interpolation parameter Y_g. k_{rgm} and Y_g involves rock properties, P and GTR. k_{rgb}, Equation (A.5), also includes the tabulated experimentally measured values of $(k_{rgb})_{meas}$ as a function of GTR.

In the core experiments, the pressure difference measured at any fractional flow of the two phases is reported at an average pressure, $(P_{ave})_{meas}$. This pressure is the arithmetic average pressure between the inlet and outlet pressure. The fluid properties are estimated at $(P_{ave})_{meas}$,

which are then used together with the pressure difference for k_r calculation of each phase. The k_r calculation is performed using the Darcy law, Equation (2).

The resulting set of highly non-linear partial differential equations (PDE) and the confining boundary conditions are solved iteratively using the Femlab finite element package. Lagrange-Quadratic elements were selected to ensure the error associated with results is less than 1%. The simulation starts with an initial guess for the two main independent variables, P and GTR, and the closer these guessed values are to the true solution the faster the iterative procedure converges. The initial guesses are $(P_{ave})_{meas}$ and the inlet value of gas fractional flow (GTR_{in}). $(P_{ave})_{meas}$ and GTR_{in} are also the input values, which together with an assumed pressure difference (ΔP) give the required boundary values (i.e., outlet pressure, total composition and inlet velocities). That is, $(P_{ave})_{meas}$ and ΔP give the outlet and inlet pressure values (i.e., P_{out} and P_{in}, respectively). GTR_{in} and fluid properties at the assumed P_{in} gives the mass flow rate (inlet velocity) and the total composition.

When the simulation has converged, the fixed P_{out} and new P_{in} estimated by the model, $(P_{in})_{mod}$, which is an average areal pressure at the inlet, are used for calculating new values of P_{ave} and ΔP. This extra round of iteration is continued till the difference between $(P_{ave})_{mod}$ and $(P_{ave})_{meas}$ and that between two consecutive $(P_{in})_{mod}$ values are within the acceptable tolerance range (less than $\pm 0.1\%$). However, to ensure faster convergence, the initial guess of P and GTR for the current round of simulation is the solution from the last round of simulation.

3.8. MODEL RESULTS

First, experiments conducted on two unperforated core samples, i.e., Clahach and Texas Cream, were simulated.

Figure 6 is the plot of pressure difference across the Clashach core sample at the three different velocity levels, measured in the laboratory and estimated by the model. The results indicate that the deviations between the measured and predicted pressure differences are reasonable. The deviation is less at lower velocity values as k_{rg} values at the lowest velocity are the input $(k_{rgb})_{meas}$ values whereas at higher velocities the k_{rg} values are calculated using the implemented k_{rg} correlation, hence an additional error is introduced. The deviations in Figure 6 at higher velocities were verified to be within the error band of k_{rg} correlation. The same findings were observed for measurements at other IFT values.

Figure 7 compares the corresponding k_{rg} values in the same experiment, calculated by writing Darcy's equation for the perforated rock, using the pressure difference across the core together with the fluid properties at the

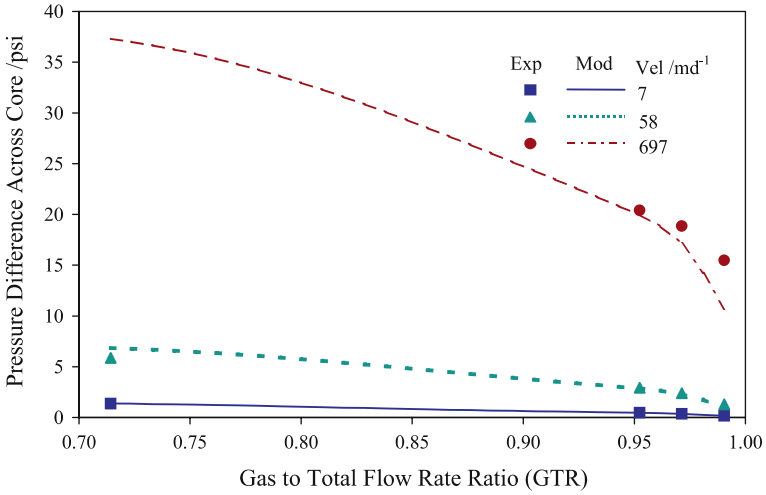

Figure 6. Measured and predicted pressure difference across Clashach core at IFT = 0.85 mN m^{-1} and three velocity levels.

average test pressure. Similarly to the findings in Figure 6, there are hardly any differences between the results of core experiments and those estimated by the model at the first velocity level. At the other two velocity levels the differences are more pronounced, but they were confirmed to be in the range of accuracy of the k_{rg} correlation. It should also be remembered that in this model k_{rL} is tied to k_{rg} by the definition of fractional flow hence, their accuracy is similar (see Figure 3(b)). Similar findings were observed in the tests conducted on Texas cream, as shown in Figure 8. These results demonstrate that the model properly solves all the governing equations describing the two-phase flow of gas and condensate including phase change and velocity effects.

The model was then used to simulate the experiments conducted on the perforated Texas cream core. Figure 9 is a plot of pressure difference across the perforated Texas Cream core sample measured experimentally and predicted by the model at three velocity levels. The model clearly underestimates the pressure difference across the core relative to the measured ones at all velocity and GTR values tested. This is believed to be due to the damage caused by the perforation process, which was not accounted for in the mathematical model.

Therefore the model was further developed to include a sub-region, whose physical properties have been uniformly damaged due to the perforation process. The integrity of the procedure was verified by successfully predicting the same result as that of one region if the same physical properties, as those of the virgin formation, were assigned to this sub-region. The unknown physical properties of the crushed zone affecting flow are the

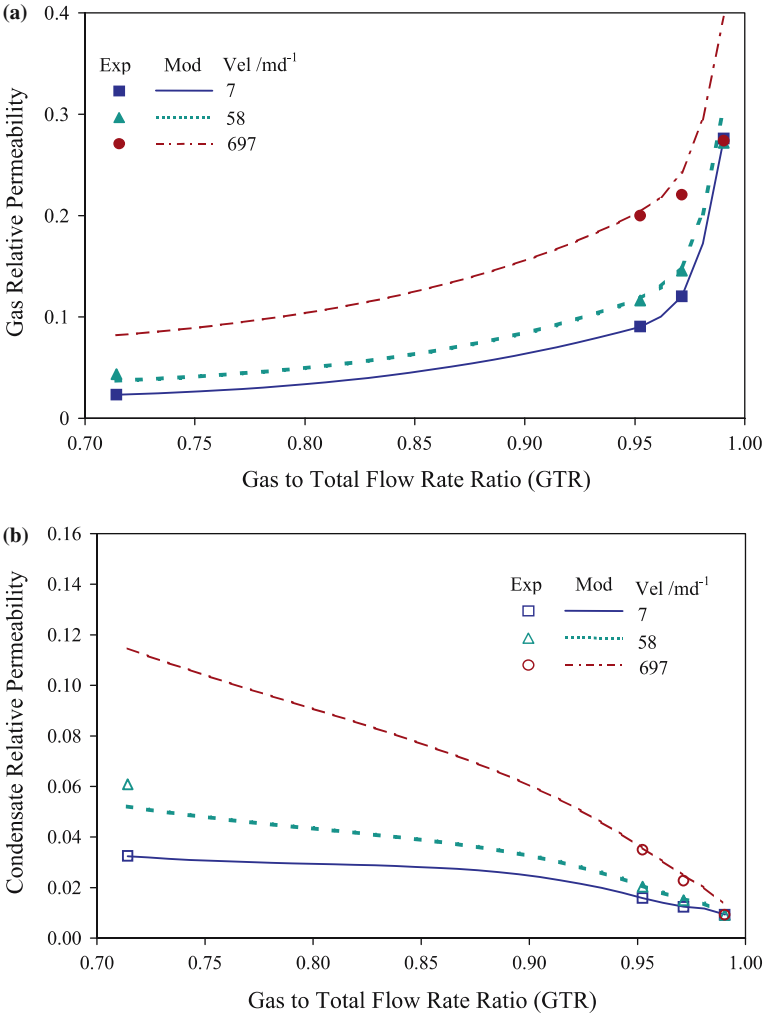

Figure 7. Measured and predicted relative permeability of Clashach core at IFT = 0.85 mN m^{-1} and three velocity levels, for (a) gas (b) condensate.

thickness, permeability and inertial factor. The single-phase flow data can be used to determine these properties. For a selected crushed zone thickness h_{cr}, the measured single-phase permeability without inertia (absolute permeability) is matched to fix the permeability of the damage zone, k_{cr}. The single-phase inertial factor for the crushed zone, β_{cr}, is then linked to porosity, ϕ_{cr}, and permeability using Geertsma's correlation (1974), which when written for both the crushed zone and the virgin formation and dividing the two gives,

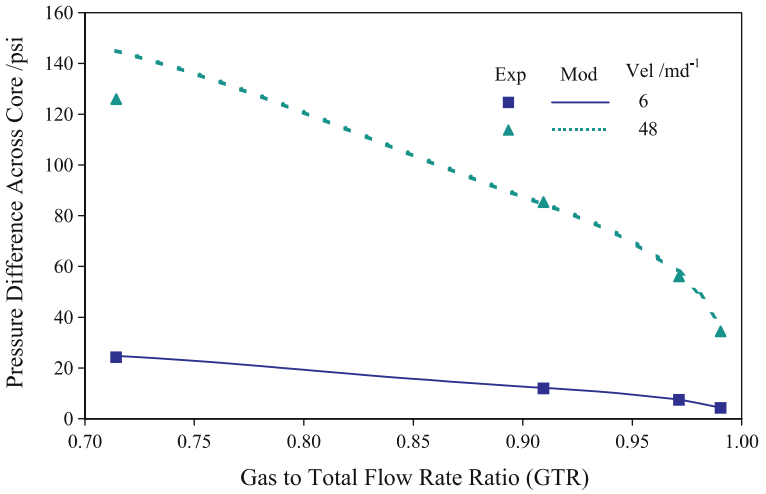

Figure 8. Measured and predicted pressure difference across Texas Cream core at IFT = 0.85 mN m^{-1} and two velocity levels.

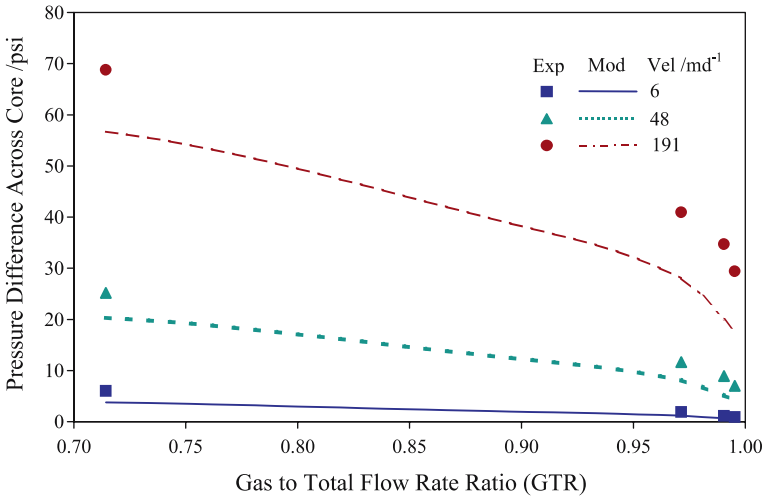

Figure 9. Measured and predicted pressure difference across the perforated Texas Cream core sample measured at IFT = 0.85 mN m^{-1} and three velocity levels with no damaged zone.

$$\frac{\beta_{cr}}{\beta} = \left(\frac{k_{cr}}{k}\right)^{-0.5} \left(\frac{\phi_{cr}}{\phi}\right)^{-5.5}, \tag{11}$$

where subscript (cr) refers to the value of the quantity for the crushed zone.

In this exercise for any given values of h_{cr} and k_{cr} the porosity, which gives the lowest devaiation between the predicted and measured permeability values at all rates that are affected by inertia, is selected as the optimum

Table I. The deviation of predicted pressure drop and gas relative permeability of the perforated Texas Cream core from measured data at different crushed zone physical properties

Index	h_{cr}/cm	k_{cr}/k	ϕ_{cr}/ϕ	AAD%-ΔP	AAD%-k_{rg}	Constants of Eq. (12)
(a) thickness-permeability-porosity $(k-\phi-h)$						
1	0.3	0.0704	0.65	16.4	17.2	0.174
2	0.2	0.0500	0.65	16.4	17.3	0.174
3	0.1	0.0271	0.60	16.4	17.3	0.176
4	0.05	0.0142	0.55	16.4	17.3	0.177
5	0.03	0.0087	0.55	16.6	17.4	0.178
(b) thickness-permeability $(k-h)$ values						
1	0.3	0.0564	1.0	14.7	17.2	0.139
2	0.2	0.0397	1.0	14.7	17.3	0.138
3	0.1	0.0212	1.0	14.6	17.3	0.138
4	0.05	0.0110	1.0	14.6	17.3	0.137
5	0.03	0.0067	1.0	14.5	17.4	0.137

value. A simpler approach is to relate the inertial factor to permeability only, and determine the damaged permeability by match all single-phase flow data in a single optimisation exercise. We evaluated the impact of the two approaches on the results of the gas-condensate flow system under study. Table 1 demonstrates that the deviations of predicted values for the two $h-k-\phi$, Table 1a, and $h-k$ sets, Table 1b are almost the same. A comparison of the average absolute deviations (AAD%) in Tables 1(a) and (b) indicates that neglecting the porosity damage results in a slight reduction in error values, which is mainly attributed to the effect of change of physical properties on the implemented k_r-correlation. The assumption of no damage results in deviations of 34.9% and 50.3% in predicted pressure drop and gas relative permeability respectively.

It should be noted that assuming radial flow through the damaged zone, the set of damaged permeability-thickness could be estimated from

$$\frac{k_{cr}}{\ln(1+h_{cr}/R_p)} = \text{constant}, \tag{12}$$

where the constant can be determined by matching the single phase flow data. The last columns in Table 1a and 1b demonstrate that this is a reasonable assumption and Equation (12) can give the set of damaged permeability-thickness with reasonable accuracy compared to numerical simulation conducted using single-phase flow data. However it should be noted Equation (12) is more suitable for $h-k$ sets in Table 1b with less

deviation compared to $h-k-\phi$ sets in Table 1a whereby the value of constant has been affected by porosity damage.

Figure 10 compares the results of the model with at a damaged thickness of $h_{cr}=0.3\,\text{cm}$ with measured values at all velocity levels. The corresponding k_{cr} and ϕ_{cr} values are those of the case indexed (1) in Table 1a, (i.e., $k/k_{cr}=0.0704$, $\phi_{cr}/\phi=0.65$). In this Figure there is also an extra plot corresponding to the case when the tip of perforation is totally closed at a velocity of $191\,\text{md}^{-1}$. This set of data demonstrates that the model correctly predicts a higher pressure-drop for the case of closed-tip perforation compared to open-tip. However, the difference between the two cases is around 1.5%, which is negligible. The same finding was observed for other intermediary velocities not shown in Figure 10. The same trends were observed for measurements at IFT of 0.15, Figure 11. It should be noted that the differences between the measured and predicted values are more pronounced compared to those at the base IFT of $0.85\,\text{mN m}^{-1}$ but they are still within the range of accuracy of the k_{rg} correlation at this IFT value.

Figure 12 displays contours of P and the arrows showing the flow lines with pressure gradient components (representing velocity value) in the r and z directions as its coordinates. There are three plots corresponding to (a) the crushed zone has the same physical properties as the virgin formation; (b) the physical properties of the damaged zone are the values of the case indexed (1) in Table 1b with the tip of perforation fully open; (c) similar to case b, but the tip of perforation is totally closed. All these three plots are the results of the model at a velocity of $191\,\text{md}^{-1}$ and GTR of 0.7143. In this Figure the core inlet is situated at the top of each plot and the white rectangular area is the perforated section drilled out of the core. The axis extending from left to right on the plots is the r-axis, representing the variation of the parameter of interest from the centre of the core along its radius at any cross-section along the axis of the core. The axis extending from bottom to top is the z-axis, representing the variation of the parameter of interest from outlet to inlet along its axis at any given radius. As it was mentioned in the previous section due to the symmetry of the core sample rotating this image by 360 degrees depicts the full 3D core.

It should be noted that there is one order of magnitude difference between the scales of the two axes in Figure 12, hence the area around perforation for the plots of Figure 12 has been magnified as shown in Figure 13. From the pressure profile and flow lines one can conclude that little flow occurs in the part towards the exit away from the tip of perforation, $0<z<0.1$. Furthermore, there is no sudden or significant pressure drop as fluids enter the perforation tunnel and as a result one can safely assume that the temperature change due to the Joule–Thomson effect is minimal.

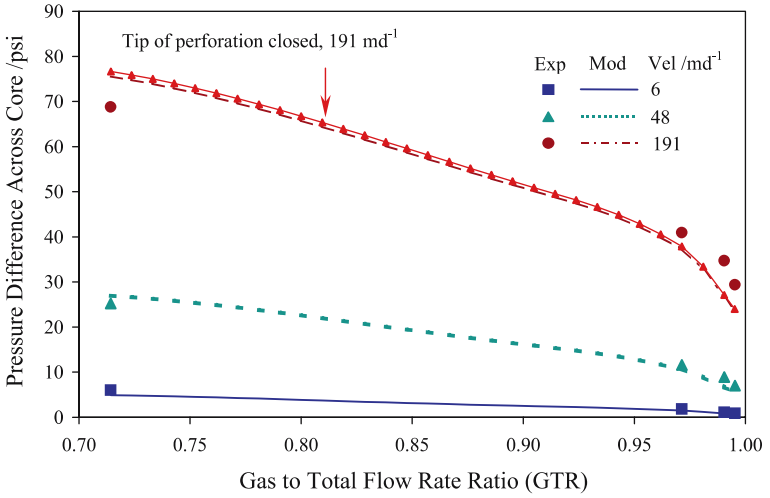

Figure 10. Pressure difference across perforated Texas Cream core sample measured in the laboratory and estimated by the model at IFT = 0.85 mN m^{-1} and three velocity levels with the damaged zone properties case one Table 1a.

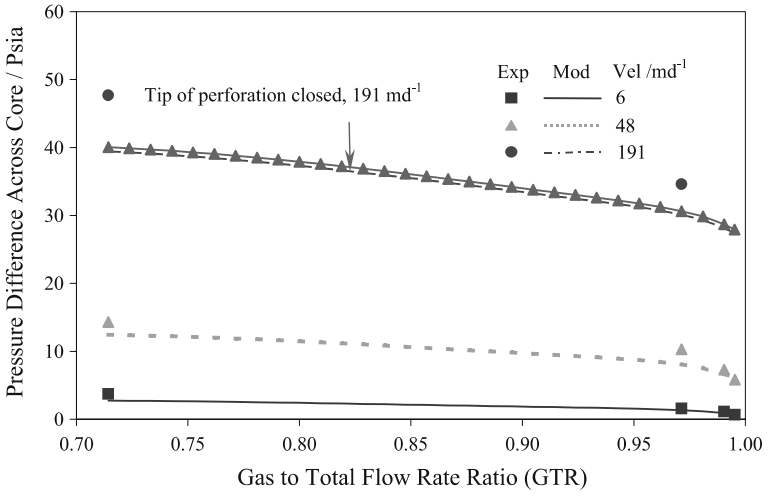

Figure 11. Pressure difference across perforated Texas Cream core sample measured in the laboratory and estimated by the model IFT = 0.15 mN m^{-1} and at three velocity levels with the damaged zone properties case one Table 1a.

When physical properties of the sub-region around the perforation are impaired, Figures 12(b), (c) and 13(b), (c) show that bigger changes occur in this region. Some form of discontinuity is noticed in the profiles between the two regions due to major differences between their physical properties. The experimentally measured pressure difference for this case was 474 kPa whilst in Figure 12(a) this value is estimated to be 395 kPa and in

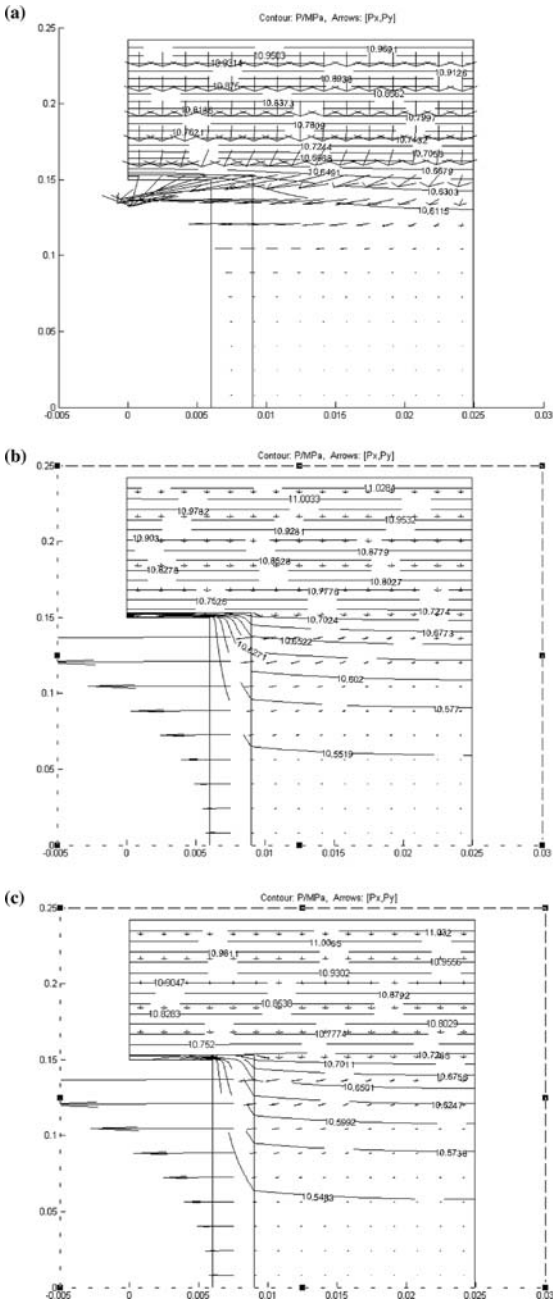

Figure 12. Distribution profile of pressure and flow lines in the model at $IFT = 0.85\,mN\,m^{-1}$, Velocity $= 191\,md^{-1}$ and $GTR = 0.7143$ for cases of: (a) the damaged zone has the same physical properties as the virgin formation; (b) the physical properties of the damaged zone are the values of case number one in Table 1 with the tip of perforation fully open; (c) similar to case (b) but the tip of perforation totally closed.

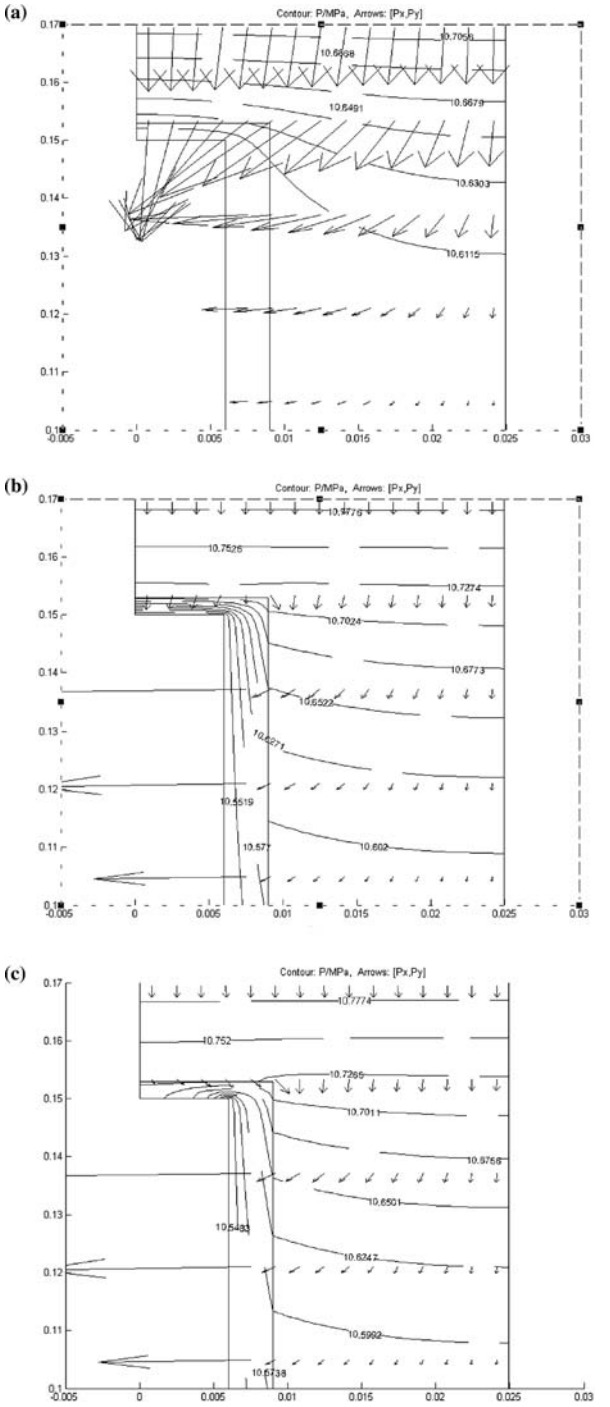

Figure 13. Distribution profile of pressure and flow lines around perforation in the model for the data of Figure 12.

Figure 12(b) this value is raised to 527 kPa, which is much closer to the measured value. The corresponding value, when the tip of the perforation was totally closed, Figure 12(b), increased slightly to 534 kPa. The corresponding profiles remained almost the same except for flow diversion near the tip of the perforation as shown in Figure 13c.

In summary, it can be concluded that two-phase flow of gas and condensate in a perforated core can be successfully simulated by considering a damaged zone with uniformly altered physical properties, which are determined by matching the results of single-phase flow. It is also important to highlight that although the k_{rg} correlation implemented in the model was originally developed for unperforated cores, nevertheless it is adequately providing k_{rg} values for the perforated core.

4. Conclusions

Using a finite element modelling approach, flow of gas and condensate around a perforation tunnel (including the damaged zone) was studied by both performing steady-state core experiments and simulating the results numerically. The model allows for the changes in fluid properties and accounts for the coupling and inertial effects using a fractional flow based correlation.

The integrity of the model has been successfully demonstrated by comparing the predicted gas and condensate flow performance for unperforated Clashach and Texas Cream core samples with the corresponding experimental observation. The deviations between the predicted and measured relative permeability values were in the range of accuracy of the implemented relative permeability correlation. The model was also used for predicting some relative permeability values for a perforated Texas Cream core sample including the damaged zone. The estimated values were lower compared to the measured values if physical properties similar to those of the virgin formation were assigned to the sub-region around perforation. However, when a damaged sub-region was considered by uniformly impairing its physical properties more realistic results were obtained. The results indicated that different sets of thickness-permeability-porosity ($h - k - \phi$) or thickness-permeability ($h - k$) values obtained from matching single-phase flow performance including inertial flow could be assigned to the uniformly damaged zone around perforation to represent the two-phase flow performance.

The status of the tip-end of the perforation for two extreme cases of totally closed and fully open was investigated and found to have minimal effect on the performance of the system.

Appendix. Relative Permeability Expression

In this section a summary of the k_r correlation used in the current work is presented. The gas relative permeability, k_{rg}, is interpolated between the base curve and the miscible-fluids curve using an interpolation function Y_j

$$k_{rg} = Y_g k_{rgb} + (1 - Y_g) k_{rgm}. \tag{A.1}$$

The miscible and the base curve in Equation (A.1) are based on the fractional flow, as the main variable. The fractional flow definition used in this study is the ratio of gas rate to total flow rate (GTR) expressed as

$$\mathrm{GTR} = \frac{Q_g}{Q_g + Q_L} = \frac{\left[\frac{k_r}{\mu}\right]_g}{\left[\frac{k_r}{\mu}\right]_L + \left[\frac{k_r}{\mu}\right]_g}. \tag{A.2}$$

Solving the above equation for k_{rL} gives

$$k_{rL} = \left[\frac{\mu_L k_{rg}}{\mu_g}\right]\left[\frac{1 - \mathrm{GTR}}{\mathrm{GTR}}\right]. \tag{A.3}$$

Therefore, when k_{rg} is determined as a function of GTR this equation automatically gives the corresponding k_{rL} at the same GTR.

The base curve, k_{rgb}, is measured at a high value of interfacial tension and low velocity (commonly measured data), $(k_{rgb})_{meas}$, which is then adjusted for the effect of inertia using the following equation:

$$\left(k_{rgb}\right)_{iner} = \left(\frac{\left(k_{rgb}\right)_{meas}}{1 + \frac{\beta \rho_{ave} k \left(k_{rgb}\right)_{meas}}{\mathrm{GTR}\mu_g} |V|_T}\right). \tag{A.4}$$

ρ_{ave} is the density value averaged based on the fractional flow of the two flowing phases.

The miscible gas relative permeability curve, which is modified to include the inertial effect, is calculated as follows:

$$k_{rgm} = \left(\frac{2GTR}{1 + \sqrt{1 + 4\beta\rho_m \left(\frac{k}{\mu_m}\right)^2 |\nabla P|}}\right). \tag{A.5}$$

In Equation (A.5) the required miscible fluid properties (i.e., density, ρ_m, and viscosity, μ_m) are the arithmetic average between the fluid properties of gas and liquid at any given pressure, in the vicinity of the miscible pressure.

It should be noted that although Equations (A.4) and (A.5) are for $S_{wi} = 0$, the same relations are valid for $S_{wi} > 0$, with $k_{eg}(S_{wi})$ and $\beta_g(S_{wi})$ replacing k and β, respectively. The interpolation parameter Y_g mainly depends on the rock properties (i.e., k, ϕ and β), interfacial tension (IFT), pressure gradient, GTR and the base capillary number as described elsewhere (Jamiolahmady *et al.*, 2003).

Acknowledgements

The above study has been sponsored by The UK Department of Trade and Industry, BP Exploration Operating Company Ltd, Gaz de France, Marathon Oil UK, Statoil A.S.A. and Total Exploration UK plc, which is gratefully acknowledged. G. Henderson and S. Ireland are thanked for conducting the relative permeability measurements.

References

Behie, A. and Settari A.: 1993, Perforation design models for heterogeneous, multiphase flow, *SPE* 25901, pp. 591–602, Proceedings of SPE RMR/Low Permeability Reservoir Symposium, Denver, Colorado, USA.

Bell, W. T., Brieger E. F. and Harrigan J. W.: 1972, Laboratory flow characteristics of gun perforations, *J. Petrol. Technol.* **24**(2), 1095–1103.

Brooks, J. E.: 1997, A simple method for estimating well productivity, *SPE* **38148**, pp. 57–64, Proceedings of SPE EFDC, The Hague, The Netherlands.

Chen, H. L., Wilson, S. D. and Monger-McClure T. G.: 1997, Determination of relative permeability and recovery for North Sea gas-condensate reservoirs, *SPE Reservoir Evaluation & Engineering* **2**(4), 393–402.

Danesh, A., Khazam, M., Henderson, G. M., Therani, D. H. and Peden, J. M.: June 1994, Gas condensate recovery studies, DTI Improve Oil Recovery and Research Dissemination Seminar, London.

Dogulu, Y. S.: 1998, Modelling of productivity in perforated completions, *SPE* **51048**, pp. 109–117, Proceedings of SPE ERM, Pittsburgh, Pennsylvania, USA.

Egan, F.: 1984, A finite element analysis of steady-state darcy and non-Darcy oil flow towards perforated wells, M.Sc. Thesis, University College.

Femlab Multiphysics Reference Manuals by COMSOL Inc., June 2002, version 2.3.0.145.

Forchheimer, P.: 1914, *Hydraulik*, Leipzig, Berlin, pp. 116–118.

Geertsma, J.: 1974, Estimating the coefficient of inertial resistance in fluid flow through porous media, *SPEJ* **14**, 445–450.

Harris, M. H.: 1966, The effect of perforating on well productivity, *J. Petrol. Technol.* **18**, 518–528, also in Petroleum Transactions AIME 237.

Henderson, G. D., Danesh, A., Tehrani, D. H., Peden, J. M.: 1996, Measurement and correlation of gas condensate relative permeability by the steady-state method, *SPEJ*, 191–201.

Henderson, G. D., Danesh, A., Tehrani, D. H.: 2001, Effect of positive rate sensitivity and inertia on gas condensate relative permeability at high velocity, *Petrol. Geosci.* **7**, 45–50.

Hong, K. C.: 1975, Productivity of perforated completions in formations with and without damage, *J. Petrol. Technol.* **27**(2), 1027–1038, also in Petroleum Transactions AIME 259.

Ichara, M. J.: 1987, The performance of perforated completions in gas reservoirs, SPE **16384**, Proceedings of SPE CRM, Ventura, California, USA, pp. 567–586.

Jamiolahmady, M., Danesh, A., Tehrani, D. H. and Duncan, D. B.: 2000, A mechanistic model of gas-condensate flow in pores, *Transport Porous Media* **41** (1), 17–46.

Jamiolahmady, M., Danesh, A., Tehrani, D. H. and Duncan, D. B.: 2003, Positive effect of flow velocity on gas-condensate relative permeability: network modelling and comparison with experimental results, *Transport Porous Media* **52** (2), 159–183.

Jamiolahmady, M., Danesh, A., Henderson, G. D., Tehrani, D. H.: 2003, Variations of Gas-Condensate Relative Permeability with Production Rate at Near Wellbore Conditions: A general Correlation, *SPE* **83960**, Proc. SPE OEC, Aberdeen, UK.

Jamiolahmady, M., Danesh, A., Sohrabi, M. and Duncan, D. B.: 2004, Flow around a rock perforation surrounded by damaged zone: Experiments vs. Theory, Submitted for publication to *J. Petrol. Sci. Engng*.

Jamiolahmady, M., Danesh, A. and Duncan, D. B.: July 2005, An improved understanding of positive velocity dependency of gas-condensate relative permeability: a mechanistic approach, in: *Proceedings of 7th World Congress of Chemical Engineering*, Glasgow, UK.

Locke, S.: 1981, An advanced method for predicting the productivity ratio of a perforated well, *J. Petrol. Technol.* **33**(2), 2481–2488.

Matlab Reference Manuals by the MathWorks Inc., May 2003, version 6.5.

McDowell, J. M. and Muskat, M.: 1950, The effect on well productivity of formation beyond perforated casing, Petroleum Transactions AIME **189**, 309–312.

McLeod, H. O.: 1983, The effect of perforating conditions on well performance, *J. Petrol. Technol.* **35**(1), 31–39.

Muskat, M.: 1943, The effect of casing perforations on well productivity, *Petroleum Transactions AIME* **151**, 175–187.

Sage, B. H., Hicks, B. L., and Lacey, W. N.: 1940, Phase equilibria in hydrocarbon system-The Methane-n-Butane systems in the two-phase region, *Ind. Eng. Chem.* **32**, 1058–1092.

SUPERTRAPP (NIST Thermophysical Properties of Hydrocarbon Mixture Database) User's Guide by National Institute of Standards and Technology (NIST), NIST Standard Reference Database 4, July 1992, version 1.0.

Weinaug, C. F. and Katz, D. L.: 1943, Surface Tension of Methane-Propane Mixtures, *Industrial Engineering Chem.* **35**(2), 239–246.

Saleh, A. M. and Stewart G.: 1996, New approach towards understanding of near well bore behaviour of perforated completions, *SPE* **36866**, pp. 447–464, Proceedings of SPE EPC, Milan, Italy.

Tariq, S. M.: 1987, Evaluation of flow characteristics of perforations including non-linear effects with the finite element method, *SPE Prod. Engng.* **2**, 104–112.